UV-activated ultrasensitive and fast reversible ppb NO_2 sensing based on ZnO nanorod modified by constructing interfacial electric field with In_2O_3 nanoparticles

Hongtao Wang, Linsheng Zhou, Yueying Liu, Fengmin Liu*, Xishuang Liang, Fangmeng Liu, Yuan Gao, Xu Yan, Geyu Lu*

State Key Laboratory on Integrated Optoelectronics, College of Electronic Science and Engineering, Jilin University, 2699 Qianjin Street, Changchun 130012, China

ABSTRACT

The poor recovery characteristic of NO_2 sensors operated at room temperature is always a challenge to solve. In order to realize the combination of ultra-high response and fast response and recovery speed, heterogeneous interfacial electric fields are constructed by loading In_2O_3 nanoparticles on ZnO nanorods, which possess fast charge transfer ability, to improve the separation efficiency of photogenerated carriers. The sensing results show that 10 mol% In_2O_3-decorated ZnO (In: Zn) exhibits a response of 117.0 to 700 ppb NO_2 at room temperature under ultraviolet (UV) illumination. Even when the concentration of NO_2 drops down to 50 ppb, the response also can reach 1.5. In addition, the sensor's response time is 100 s when exposed to 700 ppb NO_2 and can recover 90 % resistance variation within 31 s. Moreover, the role of photogenerated carriers in NO_2 sensing process under UV illumination were described in detail.

1. Introduction

As a toxic gas, NO_2 can severely harm industries, especially agriculture, and can threaten human health [1,2]. According to the American Conference of Governmental Industrial Hygienists and Occupational Safety and Health Administration, the threshold limit value and permissible short-term exposure (< 15 min) of NO_2 are 3 and 1 ppm, respectively [3–5]. Therefore, the detection of sub-ppm level NO_2 appears to be important for environment monitoring and human health.

NO_2 sensors based on metal oxide semiconductors have received extensive attention and research in recent years because of their cost-effective synthesis process and excellent sensing performance [6,7]. Among them, ZnO, as a typical n-type metal oxide semiconductor, is the most promising sensing material for detecting NO_2 gas due to its diverse morphologies [8–10], nontoxicity [11], high mobility of conduction electrons [12], and good thermal and chemical stability [13]. However, most of these sensors must be heated to 150–300 °C to provide sufficient energy for the gas adsorption and the sensing reaction with test gases, and the high operation temperature often brings serious safety problems, especially when explosive and flammable gases are present. Furthermore, continuous high temperature operation can also lead to

high power consumption and cause sensitivity drift, which seriously hinders the development of sensor assembly, wearable devices and miniaturization and integration [14,15].

Strategies for detecting harmful gases via UV activation at room temperature have been proposed in recent years [16,17]. For example, Hu et al. successfully constructed RGO/CeO_2 hybrid heterostructure and realized NO_2 gas detection at room temperature via UV light excitation [18]. Therefore, using UV light excitation instead of the traditional heating method is an effective approach to detect harmful gases at room temperature. However, room temperature NO_2 sensors still possess many drawbacks. Table 1 shows the sensing performance of NO_2 sensors operated at room temperature in recent years. The sensing performance of NO_2 sensors indicates that the poor sensitivity and the lengthy response and recovery time are still urgent problems that restrict the development of NO_2 gas sensors.

Constructing heterostructures has been demonstrated to be an effective approach to improve the gas-sensing performance. It not only results in a high surface area and synergistic effect; but also promotes the separation and transformation of photogenerated charge carriers when exposed to UV light [31,32]. In_2O_3, a typical n-type semiconductor (direct/indirect ~3.6 eV/2.8 eV, respectively), has been proved as an ideal functional sensing material for oxidizing gases such

Table 1
The sensing performance of NO_2 sensors operated at room temperature.

Materials	NO_2(ppm)	Response	T_{res} and T_{rec}[a]	Excitation source	Ref
Pt/In_2O_3	1	24	> 300 and > 300 s	no	[19]
RGO/Fe_2O_3	1	2.5	126 and 1800 s	no	[20]
PbSe QDs	50	22	7 and 39 s	no	[21]
SnO/SnO_2	1	4.5	57 and 300 s	no	[22]
$CuInS_2$ QDs	50	18	300 and > 3600 s	no	[23]
SnO_2/RGO	1	5	14 and 190 s	no	[24]
In_2O_3	50	219	89 and 80 s	365 nm LED (1.2 mW/cm^2)	[25]
GaN	100	37	250 and 1300 s	365 nm LED (no given)	[26]
PSS/ZnO	2	7	300 and 440 s	265 nm LED (0.5 mW/cm^2)	[27]
RGO/GeO_2	10	4.59	230 and 258 s	365 nm LED (0.25 mW/cm^2)	[18]
Au/MoS_2	2.5	30	~300 and 1000 s	365 nm LED (no given)	[28]
Pd/SnO_2	5	8	5 and > 30 mins	365 nm LED (35 mW/cm^2)	[29]
ZnO/In_2O_3	5	2.21	78 and 610 s	365 nm LED (25 mW/cm^2)	[30]
ZnO/In_2O_3	**0.7**	**117.0**	**100 and 31 s**	**365 nm LED (5 mW/cm^2)**	**This work**

[a] T_{res} and T_{rec} stand for response time and recovery time, respectively.

as NO_2, even at low temperature [33–35]. Furthermore, ZnO and In_2O_3 can perfectly construct the heterojunction due to the differences in the work function [36]. The benefits of using In_2O_3 nanoparticles to modify ZnO can be summarized as follows. Firstly, In_2O_3 nanoparticles are important active sites in the NO_2 atmosphere due to its excellent NO_2 sensing properties. Secondly, the interface electric field between In_2O_3 and ZnO promotes the separation of photogenerated charge carriers and increases the number of electrons participated in the sensing reaction. Therefore, it can be speculated that combining ZnO and In_2O_3 is an effective approach to detect infinitesimal NO_2.

In this work, we successfully prepared In_2O_3-decorated ZnO nanorods through a facile two-step method. The ultra-high response of ZnO/In_2O_3 composites is attributed to the excellent NO_2 sensing properties of In_2O_3, the interface electric field between ZnO and In_2O_3, and the increased oxygen vacancies. Furthermore, the one-dimensional nanorod structure greatly improves the response and recovery speed. Moreover, the influence of relative humidity (RH) (30 %–90 % RH) on sensing performance and the mechanism under UV light irradiation were also studied.

2. Experimental section

2.1. Synthesis of In_2O_3-decorated ZnO nanorod

Pure ZnO nanorods were synthesized via a facile hydrothermal route [37]. A series of 5, 10, and 15 mol% In_2O_3-decorated ZnO nanorod heterojunction composites, whose molar percentage was defined as the ratio of the moles of In to that of Zn, was synthesized via a simple chemical precipitation method. The detailed steps are as follows. First, 200 mg of as-prepared ZnO was dispersed in 25 ml of deionized water via ultrasonic treatment. Then, a certain quantity of $In(NO_3)_3 \cdot 4.5H_2O$ and 50 mg of hexadecyl trimethyl ammonium bromide (CTAB) were added into the above dispersed solution under constant stirring. Subsequently, 5 ml of 0.5 M NaOH solution was added to the mixed solution dropwise under continuous stirring. After stirring for 20 min, white precipitates were collected via centrifugation, washed with ethanol and water, and dried in an oven at 70 °C for 10 h. Finally, the product was annealed at 400 °C for 2 h at a heating rate of 10 °C/min. The fabricated samples were labeled pure ZnO, ZnO/In_2O_3-5, ZnO/In_2O_3-10, and ZnO/In_2O_3-15, respectively.

2.2. Sample characterization

The crystal structures of the samples were analyzed using a powder X-ray diffractometer (XRD) (Rigaku D/Max-2550 VX-ray diffractometer) using high-intensity Cu Kα radiation (λ = 1.5403 Å). The surface morphologies of the samples were characterized by a field

emission scanning electron microscope (FESEM, JEOL JSM-7500 F, operated at an accelerating voltage of 15 kV). Transmission electron microscopy (TEM) and high-resolution transmission electron microscopy (HRTEM) were recorded on a JEOL JSM-2100 F operating at an accelerating voltage of 200 kV. The X-ray photoelectron spectroscopy (XPS) measurements were performed in a VG ESCALAB 210 (VG Scientific, UK) photoelectron spectrometer equipped with a Mg Kα$_{1,2}$ exciting source and source power of 300 W. All the binding energies of the elements were calibrated to the carbon binding energy of 284.8 eV. The improved separation efficiency of photogenerated charge carriers was demonstrated by detection system of the surface photovoltage (SPV) measurement.

2.3. Fabrication and measurement of the gas sensor

The sensors were fabricated as previously reported article [38]. A UV-LED (λ = 365 nm, Shenzhen Xinxingyuan Photoelectric Device Co. Ltd., China) was installed on the top of the base to motivate the sensor. The light intensity (5 mW/cm^2) was measured by a light irradiation meter (UV-313/340, Zhuhai Tianchuang Instrument Company, China). Resistances of the sensors was measured by a multimeter (Fluke 8846A) and recorded in real time by a data-acquisition PC. The test system is static and the volume of gas sensing chambers is 1 L. Two gas chambers were used during the sensing test, and a certain concentration of NO_2 is pre-injected into one of the gas chambers through a microsyringe while the other gas chamber contains pure air. When the resistance stabilizes in the air, the sensor element was moved quickly to the gas chamber containing NO_2. Therefore, it does not need to consider the filling time, and the response/recovery time is a true reflection of response/recovery speed. It is important to note that there is no change in atmosphere of the gas chambers during the movement. If both gas chambers contain pure air, there will be no change in resistance. All measurements were conducted at room temperature. The gas-sensing response is defined as $S = R_g/R_a$, where R_g and R_a are the real-time resistance of the sensor after exposing to NO_2 gas and the baseline resistance in pure air. In addition, the response and recovery time is defined as the time taken by the sensor to achieve 90 % of the total resistance change.

3. Result and discussion

3.1. Material characterizations

The crystal phase of the pure ZnO and ZnO/In_2O_3 composites was confirmed via X-ray diffraction, as shown in Fig. 1. The pure ZnO exhibits eleven peaks at 31.7°, 34.4°, 36.2°, 47.5°, 56.7°, 62.9°, 66.4°, 68.0°, 69.1°, 72.6°, and 77.0°, corresponding to (100), (002), (101), (102), (110), (103), (200), (112), (201), (004), and (202) of the
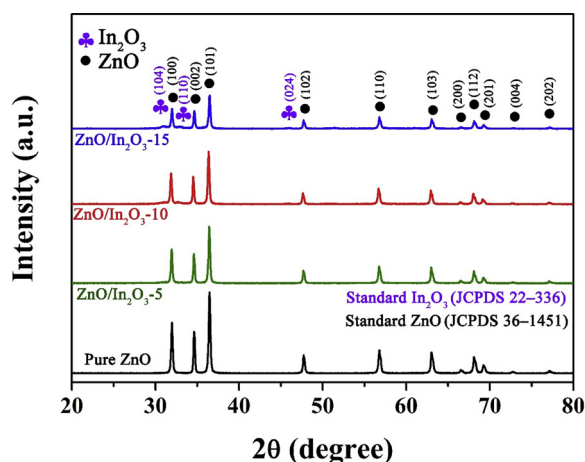
Fig. 1. XRD patterns of pure ZnO and ZnO/In$_2$O$_3$ composites.

hexagonal wurtzite ZnO, respectively (JCPDS File No. 36–1451) [39]. The diffraction peaks of ZnO are sharp and intense, indicating its high crystalline nature. With the increase in In loading, some weak diffraction peaks at 30.9°, 33.3°, and 45.9° in ZnO/In$_2$O$_3$-15 emerge, which can be assigned to (104), (110), and (024) of cubic phase In$_2$O$_3$, respectively (JCPDS File No. 22–336). Furthermore, no impurity diffraction peaks were observed.

The morphology features of pure ZnO and ZnO/In$_2$O$_3$ composites were conducted by SEM and TEM measurements, as shown in Fig. 2. The SEM image shows that the as-prepared pure ZnO consisted of nanorods, which are roughly 50–300 nm in diameter and 1–2 μm in length. Moreover, the surface of the ZnO nanorods is very smooth. Regarding ZnO/In$_2$O$_3$-10, part of the In$_2$O$_3$ nanoparticles with diameters of 20–30 nm deposit on the surface of the ZnO nanorods, whereas some agglomerate. The TEM image in Fig. 2c shows a single ZnO nanorod with some In$_2$O$_3$ nanoparticles deposit on its surface. The sizes of the In$_2$O$_3$ nanoparticles are generally consistent with the SEM results. The high-resolution TEM image in Fig. 2d confirms that the

lattice spacings are 0.250 and 0.288 nm, which are ascribed to the (101) crystal face of the hexagonal wurtzite ZnO and the (104) crystal face of In$_2$O$_3$, respectively.

An XPS analysis was performed to investigate the chemical states of as-prepared samples. Fig. 3(b–d) show the corresponding spectra of Zn 2p, In 3d, and O 1s of pure ZnO and ZnO/In$_2$O$_3$-10, respectively. The Zn 2p spectra of pure ZnO and ZnO/In$_2$O$_3$-10 show two main peaks at 1021.3 and 1044.4 eV, which correspond to the Zn 2p$_{3/2}$ and Zn 2p$_{1/2}$ electronic states, respectively. This result indicates the existence of a divalent oxidation state in the ZnO nanorods [40]. Fig. 3c exhibits the pronounced splitting of In 3d emission into two symmetric peaks. The peak centered at 452.1 eV is attributed to the In 3d$_{3/2}$ and that at 444.2 eV is attributed to In 3d$_{5/2}$, indicating the normal oxidation state of In^{3+} in ZnO/In$_2$O$_3$-10 [41]. The O 1s spectra of pure ZnO and ZnO/In$_2$O$_3$-10 are presented in Fig. 3d, and the O 1s region can be fitted into three peaks with centers at 530.1, 531.0, and 532.3 eV, respectively. The peak at 530.1 eV corresponds to the crystal lattice oxygen (Zn-O, In-O) in the composites. The peak located at 531.0 eV can be attributed to the oxygen vacancy, which has a significant effect on the sensing properties [42]. The peak at 532.3 eV can be ascribed to the chemisorbed oxygen species (H$_2$O, O$_2$) on the surface of ZnO. Table 2 shows the percentage of each component in O 1s of pure ZnO and ZnO/In$_2$O$_3$-10. It can be seen that the oxygen vacancy proportion of ZnO/In$_2$O$_3$-10 increases significantly from 23.9%–32.0% compared with that of pure ZnO. Furthermore, the atomic% of different components in pure ZnO and ZnO/In$_2$O$_3$-10 obtained by XPS analysis was shown in Table 3. For ZnO/In$_2$O$_3$-10, it can be roughly estimated the stoichiometry ratio of In to Zn is 0.43: 1, that is In$_2$O$_3$: ZnO is 0.215: 1. In this work, In$_2$O$_3$ nanoparticles are mainly distributed on the surface of ZnO, and the XPS analyzes the surface chemical composition of materials and cannot reflect the bulk chemical composition. Therefore, the XPS showed a larger ratio of In to Zn in product than that of in reactant.

SPV measurement was conducted to investigate the effect of the interface electric field between ZnO and In$_2$O$_3$ on the separation efficiency of photogenerated electron-hole pairs. It is generally accepted that the stronger SPV signal is, the better separation efficiency is [16]. For pure ZnO, SPV signal is generated by the self-built electric field in
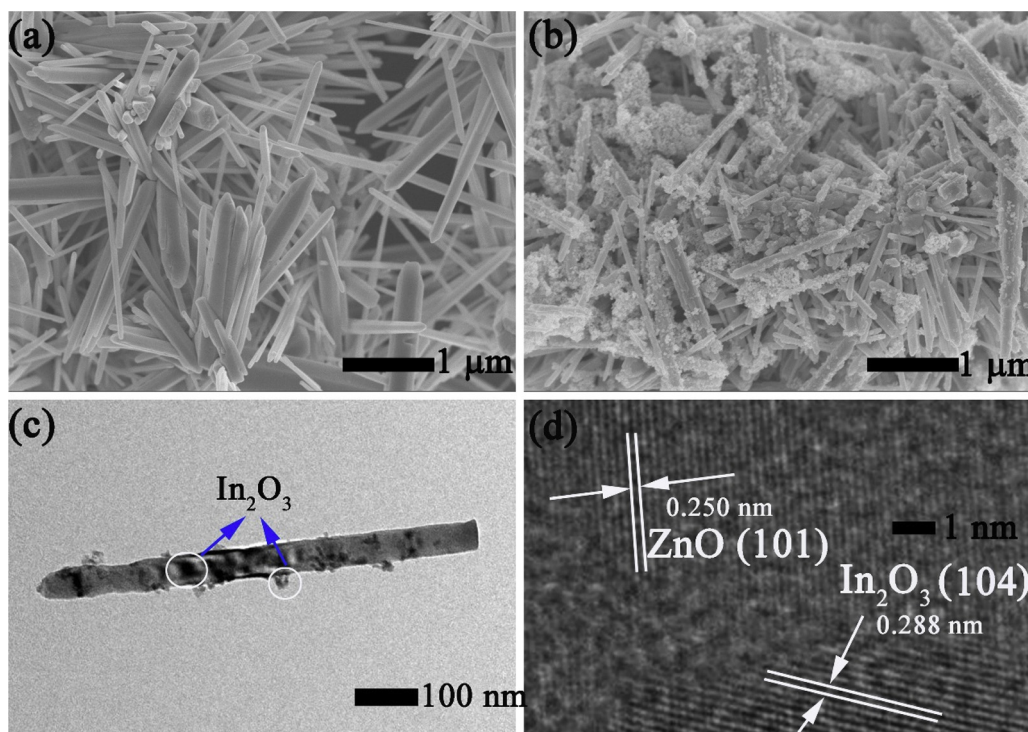

Fig. 2. (a–b) SEM images of pure ZnO and ZnO/In$_2$O$_3$-10; (c–d) low-magnification and high-magnification TEM images of ZnO/In$_2$O$_3$-10.
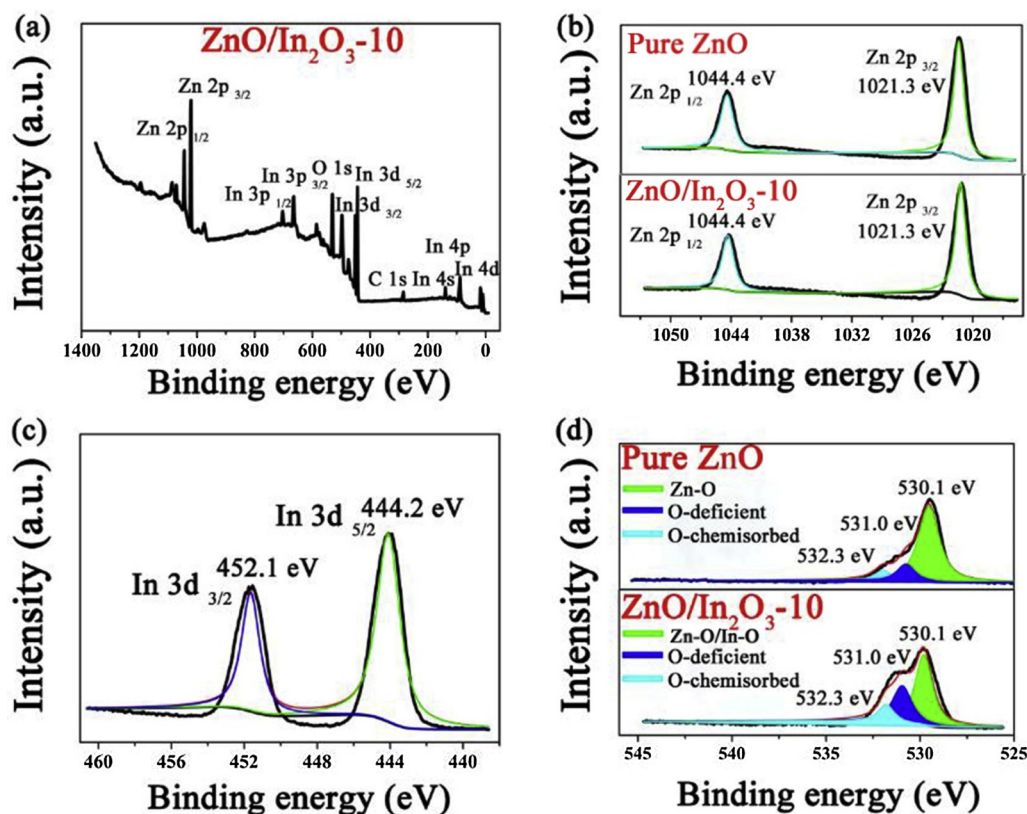
Fig. 3. (a) Survey spectra of ZnO/In$_2$O$_3$-10; high-resolution XPS spectra of (b) Zn 2p (c) In 3d (d) O 1s of pure ZnO and ZnO/In$_2$O$_3$-10.

Table 2
The composition in O 1s of pure ZnO and ZnO/In$_2$O$_3$-10.

Sample	Lattice oxygen	O-vacancy	O-chemisorbed
Pure ZnO	66.4 %	23.9 %	9.7 %
ZnO/In$_2$O$_3$-10	55.9 %	32.0 %	12.1 %

Table 3
Atomic% of different components in pure ZnO and ZnO/In$_2$O$_3$-10 obtained by XPS analysis.

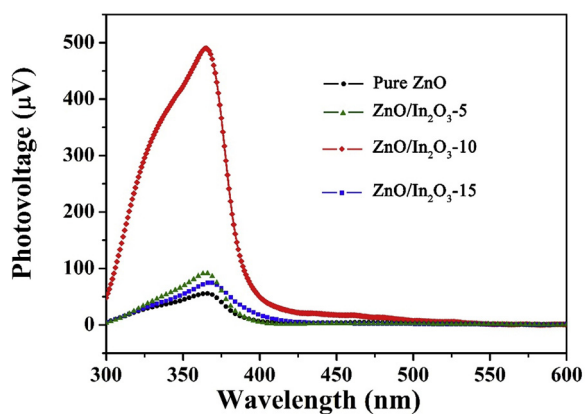| Sample	C%	In%	O%	Zn%
Pure ZnO	17.2 %	—	40.5 %	42.3 %
ZnO/In$_2$O$_3$-10	17.7 %	10.1 %	48.6 %	23.6 %

Fig. 4. SPV spectra of pure ZnO and ZnO/In$_2$O$_3$ composites.

surface space charge region. When ZnO is exposed to the air, oxygen molecules are adsorbed on the surface of ZnO to generate negative adsorbed oxygen ions. Meanwhile, a positively charged space charge region beneath the ZnO surface is produced. Thus, a self-built electric field is generated from the bulk phase to the outer surface. When ZnO is irradiated by light with a larger photon energy compared with its band gap energy, photogenerated holes will transfer to the outer surface of ZnO under the action of self-built electric field, and a positive SPV signal is obtained. For ZnO/In$_2$O$_3$ composites, the SPV signal is generated by the self-built electric field caused by adsorbed negative oxygen ions and the interface electric field between the heterojunction. Fig. 4 shows that ZnO/In$_2$O$_3$-10 exhibits the highest SPV signal at approximately 368 nm, which indicated that it has the best separation efficiency of photogenerated electron-hole pairs. As a result, more oxygen molecules can trap photogenerated electrons and adsorb on the surface of ZnO. Therefore, the stronger SPV signal means more adsorbed oxygen ions, which is benefit for the sensing reaction. In the SPV spectra, the SPV signal increases with the increase of In$_2$O$_3$ loading, indicating that the separation efficiency increases and more adsorbed oxygen ions is generated. Less loading of In$_2$O$_3$ is not enough to improve the separation efficiency to a large extent. On the contrary, excess loading of In$_2$O$_3$ creates a lot of recombination centers at the heterogeneous interface, which seriously affect the separation efficiency.

3.2. NO$_2$ sensing performance

The dynamic resistance curves with time based on ZnO/In$_2$O$_3$ composites are shown in Fig. 5(a–c). All sensors have complete response and recovery process to NO$_2$ ranging from 50 to 700 ppb, and the resistance variation gradually increased with NO$_2$ concentration. For comparison, the response curves as a function of NO$_2$ concentration were shown in Fig. 5d. It can be seen that ZnO/In$_2$O$_3$-10 exhibits higher responses than ZnO/In$_2$O$_3$-5 and ZnO/In$_2$O$_3$-15 no matter in low or high concentrations of NO$_2$. It's worth mentioning that the response of
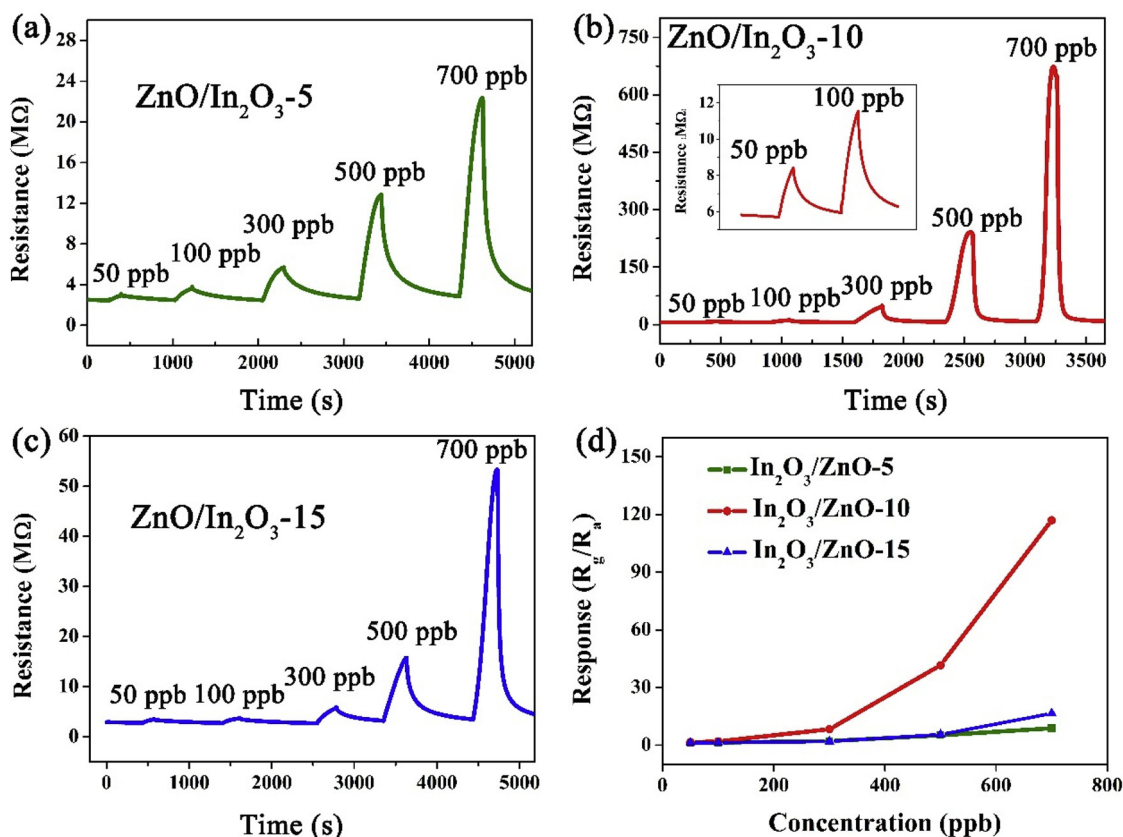
Fig. 5. (a–c) The real-time resistance curves of ZnO/In$_2$O$_3$-5, ZnO/In$_2$O$_3$-10 and ZnO/In$_2$O$_3$-15 to different NO$_2$ concentration under UV irradiation, respectively; (d) response curves of pure ZnO and ZnO/In$_2$O$_3$ composites with NO$_2$ concentration.

pure ZnO is extremely small to neglect NO$_2$ below 700 ppb. The response of ZnO/In$_2$O$_3$-10 to NO$_2$ concentrations of 50, 100, 300, 500, and 700 ppb are 1.5, 2.0, 8.3, 41.6, and 117.0, respectively. The worse sensing performance of the sensor based on ZnO/In$_2$O$_3$-5 is mainly due to the low modifier, which is insufficient to improve the separation efficiency of photogenerated electron–hole pairs effectively. On the contrary, excess loading of In$_2$O$_3$ creates a lot of recombination centers at the interface, which seriously affect the separation efficiency. Hence, ZnO/In$_2$O$_3$-10 exhibits the highest response to NO$_2$ among the as-prepared ZnO/In$_2$O$_3$ composites.

The gas-sensing properties of ZnO/In$_2$O$_3$-10 with and without UV-LED light illumination were also explored at room temperature. As shown in Fig. 6a, without UV light illumination, ZnO/In$_2$O$_3$-10 exhibits a small resistance change to 700 ppb NO$_2$ and the resistance value is difficult to revert to the original baseline after the removal from NO$_2$. In contrast, under UV light illumination, the resistance of In$_2$O$_3$/ZnO-10 changes dramatically, and the resistance value can be quickly restored to the baseline when the sensor is removed to the air due to the strong oxidizing ability of photogenerated holes. Particularly, the response of the ZnO/In$_2$O$_3$-10 sensor to 700 ppb NO$_2$ increases from 4.5 (without UV light illumination) to 117.0 (under UV light illumination), indicating that UV light greatly improves the response at room temperature. As shown in Fig. 6a, the response and recovery time is approximately 100 and 31 s to 700 ppb NO$_2$, respectively, which are superior to those of the reported NO$_2$ sensors operated at room temperature, as shown in Table 1.

A repeatable response at a certain concentration is critical for gas sensors. To evaluate the repeatability of ZnO/In$_2$O$_3$-10, we performed four continuous sensing processes in 500 ppb NO$_2$ atmosphere. As shown in Fig. 6b, no obvious decline in the amplitude of the resistance is observed after four periods, indicating that the sensor based on ZnO/In$_2$O$_3$-10 has good repeatability to a certain concentration of NO$_2$ gas.

Selectivity is another important parameter for gas sensors. To investigate the selectivity of the as-fabricated gas sensors, we have studied their sensing response to other gases, such as CO, NH$_3$, C$_6$H$_6$, H$_2$, ethanol, and acetone, in 100 ppm at room temperature under UV light irradiation. Clearly, the gas response of ZnO/In$_2$O$_3$-10 to 700 ppb NO$_2$ is much higher than those of the other gases, as shown in Fig. 6c, indicating that the gas sensor based on In$_2$O$_3$/ZnO-10 is more sensitive and selective to NO$_2$ gas.

The interference of humidity is a very tricky problem for gas sensors, especially those operated at room temperature. In recent years, some researchers have demonstrated that UV light can effectively promote the desorption of physically adsorbed water and have realized the minimum of cross-sensitivity of relative humidity [43]. To investigate the effect of humidity on the sensors, we measured the resistance changes of ZnO/In$_2$O$_3$-10 to 500 ppb NO$_2$ in RH ranging from 30 % to 90 %. As shown in Fig. 6d, the sensor resistance decreases slightly in low and moderate humidity atmosphere and exhibits a serious decrease in a high-humidity environment because excessive water molecules occupy the adsorption sites on the surface of ZnO and reduce the adsorption of oxygen. However, the response is still acceptable and the sensor still exhibits complete response and recovery process.

3.3. Sensing mechanism

Sensing response is produced by the redistribution of electrons in semiconductors in different atmospheres. At room temperature, a part of ambient oxygen molecules adsorbed on the surface of ZnO/In$_2$O$_3$ composites can capture electrons from the conduction band to form chemisorbed oxygen ion ($O_{2(ads)}^-$), as shown in the following reaction.

$$O_{2(gas)} + e^- \rightarrow O_{2(ads)}^- \tag{1}$$

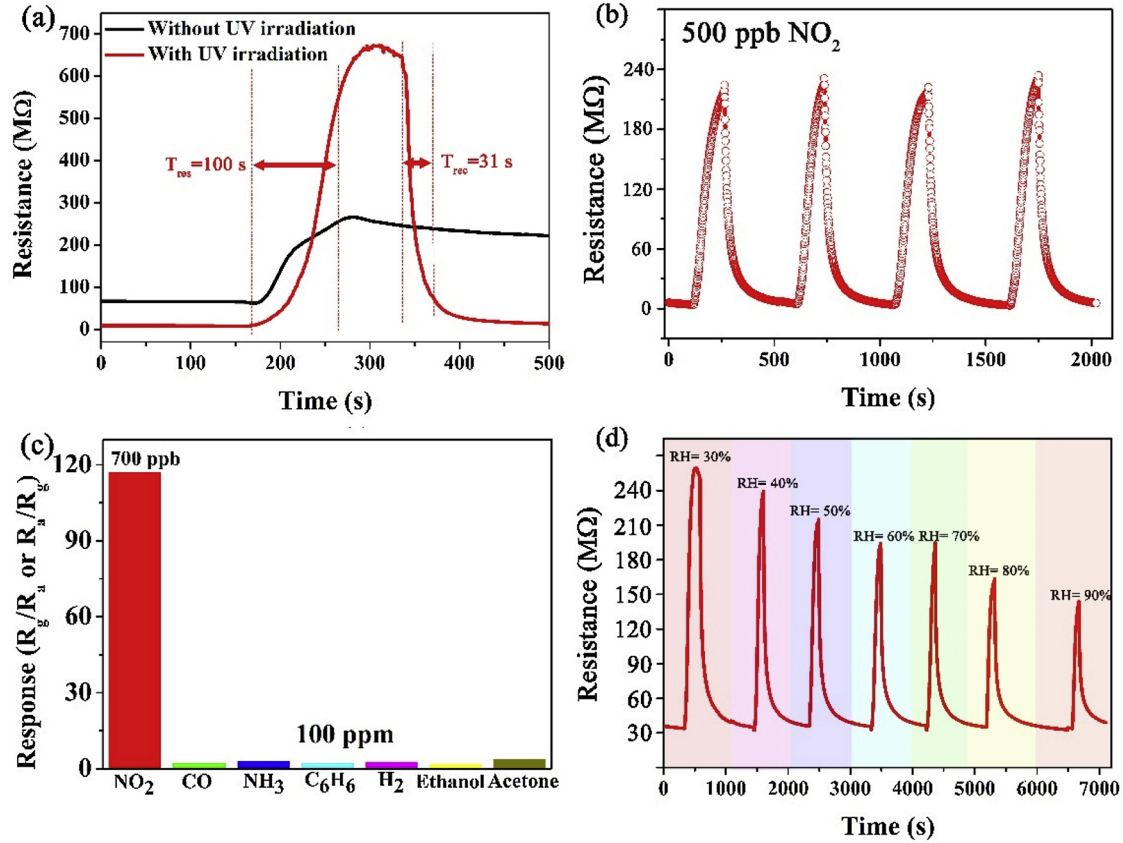Once ZnO/In$_2$O$_3$ composites are exposed to UV light,

Fig. 6. (a) The resistance changes of ZnO/In_2O_3-10 to 700 ppb NO_2 with and without UV irradiation at room temperature; (b) the response of four cycles of ZnO/In_2O_3-10 to 500 ppb NO_2; (c) the response of ZnO/In_2O_3-10 to other gases; (d) the response changes of ZnO/In_2O_3-10 to 500 ppb NO_2 at different relative humidity (30 %–90 % RH).

photogenerated electron–hole pairs are produced, as shown in the reaction.

$$h\upsilon \rightarrow e_{h\upsilon}^- + h_{h\upsilon}^+ \tag{2}$$

On the one hand, the photogenerated holes can promote the desorption of $O_{2(ads)}^-$ due to their oxidation ability. On the other hand, oxygen molecules can reattach to the surface of ZnO/In_2O_3 composites again and form photosorbed oxygen ions ($O_{2(h\upsilon)}^-$) by capturing photogenerated electrons. These processes are described in the following reaction.

$$O_{2(gas)}^- + h_{h\upsilon}^+ \rightarrow O_{2(gas)} \tag{3}$$

$$O_{2(gas)} + e_{h\upsilon}^- \rightarrow O_{2(h\upsilon)}^- \tag{4}$$

When the oxidizing gas NO_2 appears, the electron depletion layer become thicker due to the formation of $NO_{2(h\upsilon)}^-$ and $NO_{3(h\upsilon)}^-$.

$$NO_2 + e_{h\upsilon}^- \rightarrow NO_{2(h\upsilon)}^- \tag{5}$$

$$NO_2 + O_{2(h\upsilon)}^- \rightarrow NO_{2(h\upsilon)}^- + O_{2(gas)} \tag{6}$$

$$2NO_2 + O_{2(h\upsilon)}^- + e_{h\upsilon}^- \rightarrow 2NO_{3(h\upsilon)}^- \tag{7}$$

When ZnO/In_2O_3 composites are removed from NO_2 to air, the photogenerated holes can also promote the desorption of NO_2, as shown in the following reaction [28].

$$NO_{2(h\upsilon)}^- + h^+ \rightarrow NO_{2(gas)} \tag{8}$$

$$2NO_{3(h\upsilon)}^- + 2h^+ \rightarrow 2NO_{2(gas)} + O_2 \tag{9}$$

Compared with the pure ZnO, the improved response of ZnO/In_2O_3 composites can be attributed to the following factors. Firstly, the excellent NO_2 sensing properties of In_2O_3, which is important active sites

in the NO_2 atmosphere. Secondly, the improved separation efficiency of photogenerated charge carriers increases the amounts of $O_{2(h\upsilon)}^-$, which greatly promotes the reaction (6–7). The amount of $O_{2(h\upsilon)}^-$ on the surface of ZnO/In_2O_3 composites can be greatly increased due to the action of the interface electric field between ZnO and In_2O_3. When ZnO and In_2O_3 come in contact, some free electrons will transfer from In_2O_3 to ZnO until the two systems attain a new equilibrium Fermi energy level and an interfacial electric field is formed, whose direction is from In_2O_3 to ZnO [44]. The energy band of ZnO and In_2O_3 before and after contact was shown in Fig. 7a. When ZnO/In_2O_3 composites are activated by UV light, the photogenerated electrons in the conduction band of ZnO immediately flow into In_2O_3 under the action of interfacial electric field, whereas the photogenerated holes in the valence band of In_2O_3 transfer into ZnO. The separation of photogenerated electrons and photogenerated holes in space inhibits the recombination, so more oxygen molecules can capture photogenerated electrons to attach to the surface of ZnO/In_2O_3 composites. It's worth noting that although NO_2 can capture electrons from both $O_{2(h\upsilon)}^-$ and the remaining photogenerated electrons, the $O_{2(h\upsilon)}^-$ is the preferred reaction sites [45]. The variation of energy band and the structural model of ZnO/In_2O_3 composites in different atmosphere was shown in Fig. 7(b–c).

In addition, the enhancement of the response also benefits from the increase in the oxygen vacancy, which has been proven by XPS test. The increase of the oxygen vacancy increases the amount of $O_{2(ads)}^-$. Furthermly, the $O_{2(ads)}^-$ enhance the self-built electric field on the surface of ZnO/In_2O_3 composites, thus improving the separation efficiency of photogenerated electron-hole pairs.

In conclusion, the increased response of ZnO/In_2O_3 composites is attributed to the excellent NO_2 sensing properties of In_2O_3, the interface electric field between ZnO and In_2O_3, and the increased oxygen vacancies.

(a)

(b) Potential barriers between ZnO and In₂O₃

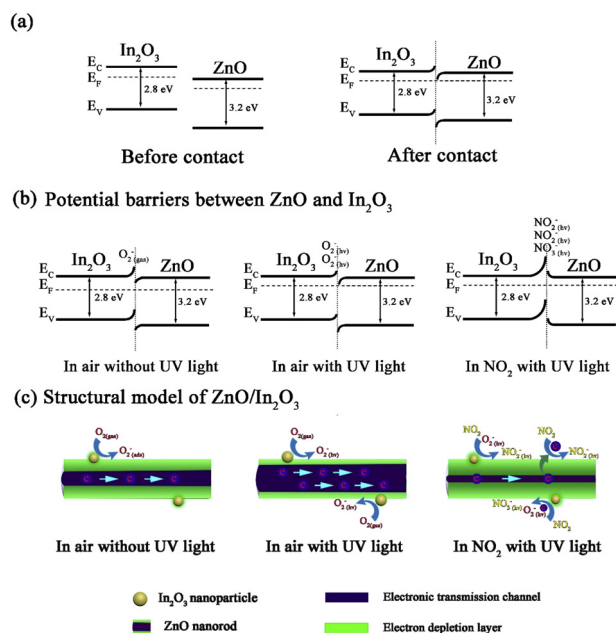**(c) Structural model of ZnO/In₂O₃**

Fig. 7. (a) The energy band of ZnO and In_2O_3 before and after contact; (b–c) the variation of energy band and the structural model of ZnO/In_2O_3 composites in different atmosphere, respectively.

As shown in Table 1, the ZnO/In_2O_3 composites also exhibits excellent response and recovery characteristic compared with other sensors operated at room temperature. The short response and recovery time are mainly due to the rod structure of ZnO. The smooth transport channels of ZnO nanorod speed up the transfer of electrons, thus quickly reflecting the resistance changes. Therefore, while displaying high response, In_2O_3 decorated ZnO nanorod also exhibits fast response and recovery rate to NO_2.

4. Conclusion

In this work, a series of ZnO/In_2O_3 composites were synthesized using a facile two-step method and characterized by XRD, SEM, TEM, XPS, and SPV. The results show that In_2O_3 nanoparticles and ZnO nanorod are in close contact and perfectly form the interface electric field. Among them, 10 mol% ZnO/In_2O_3 composites (In: Zn) exhibited the highest response (117.0–700 ppb NO_2) at room temperature under UV light irradiation (λ = 365 nm, intensity: 5 mW/cm^2). Moreover, the sensor also showed short response and recovery time of 100 and 31 s, respectively. The excellent response is attributed to the excellent NO_2 sensing properties of In_2O_3, the interface electric field between ZnO and In_2O_3, and the increased oxygen vacancies. The short response and recovery time are due to the one-dimensional nanorod structure of ZnO.

Declaration of Competing Interest

The authors declare that they have no known competing financial interests or personal relationships that could have appeared to influence the work reported in this paper.

Acknowledgements

References

[1] Z. Wang, L. Huang, X. Zhu, X. Zhou, L. Chi, An ultrasensitive organic semiconductor NO_2 sensor based on crystalline TIPS-pentacene films, Adv. Mater. 29 (2017) 1703192.
[2] A. Ebrahim, T. Bandosz, Ce(III) doped Zr-based MOFs as excellent NO_2 adsorbents at ambient conditions, ACS Appl. Mater. Interfaces 5 (2013) 10565–10573.
[3] K. Tian, X. Wang, H. Li, R. Nadimicherla, X. Guo, Lotus pollen derived 3–dimensional hierarchically porous NiO microspheres for NO_2 gas sensing, Sens. Actuators B Chem. 227 (2016) 554–560.
[4] Z. Li, Y. Liu, D. Guo, J. Guo, Y. Su, Room-temperature synthesis of CuO/reduced graphene oxide nanohybrids for high-performance NO_2 gas sensor, Sens. Actuators B Chem. 271 (2018) 306–310.
[5] E. Wu, Y. Xie, B. Yuan, H. Zhang, X. Hu, J. Liu, H. Zhang, Ultrasensitive and fully reversible NO_2 gas sensing based on p-type $MoTe_2$ under ultraviolet illumination, ACS Sens. 3 (2018) 1719–1726.
[6] J. Bang, M. Choi, A. Mirzaei, Y. Kwon, S. Kim, T. Kim, H. Kim, Selective NO_2 sensor based on Bi_2O_3 branched SnO_2 nanowires, Sens. Actuators B 274 (2018) 356–369.
[7] S. Roso, D. Degler, E. Llobet, N. Barsan, A. Urakawa, Temperature-dependent NO2 sensing mechanisms over indium oxide, ACS Sens. 2 (2017) 1272–1277.
[8] S. Agarwal, P. Rai, E. Gatell, E. Llobet, F. Güell, M. Kumar, K. Awasthi, Gas sensing properties of ZnO nanostructures (flowers/rods) synthesized by hydrothermal method, Sens. Actuators B 292 (2019) 24–31.
[9] J. Gonzalez-Chavarri, L. Parellada-Monreal, I. Castro-Hurtado, E. Castaño, G. Mandayo, ZnO nanoneedles grown on chip for selective NO_2 detection indoors, Sens. Actuators B 255 (2018) 1244–1253.
[10] R. Chen, J. Wang, L. Xiang, Facile synthesis of mesoporous ZnO sheets assembled by small nanoparticles for enhanced NO_2 sensing performance at room temperature, Sens. Actuators B 270 (2018) 207–215.
[11] F. Fan, Y. Feng, S. Bai, J. Feng, A. Chen, D. Li, Synthesis and gas sensing properties to NO_2 of ZnO nanoparticles, Sens. Actuators B 185 (2013) 377–382.
[12] X. Chen, Y. Shen, P. Zhou, X. Zhong, G. Li, C. Han, D. Wei, Li S, Bimetallic Au/Pd nanoparticles decorated ZnO nanowires for NO_2 detection, Sens. Actuators B 289 (2019) 160–168.
[13] S. Liu, B. Yu, H. Zhang, T. Fei, T. Zhang, Enhancing NO_2 gas sensing performances at room temperature based on reduced graphene oxide-ZnO nanoparticles hybrids, Sens. Actuators B 202 (2014) 272–278.
[14] W. Han, H. He, L. Zhang, C. Dong, H. Zeng, Y. Dai, L. Xing, Y. Zhang, Y. Xue, A self-powered wearable noninvasive electronic-skin for perspiration analysis based on piezo-biosensing unit matrix of enzyme/ZnO nanoarrays, ACS Appl. Mater. Interfaces 9 (2017) 29526–29537.
[15] Y. Xiong, W. Lu, D. Ding, L. Zhu, X. Li, C. Ling, Z. Xue, Enhanced room temperature oxygen sensing properties of LaOCl-SnO2 hollow spheres by UV light illumination, ACS Sens. 2 (2017) 679–686.
[16] J. Cui, L. Shi, T. Xie, D. Wang, Y. Lin, UV-light illumination room temperature HCHO gas-sensing mechanism of ZnO with different nanostructures, Sens. Actuators B 227 (2016) 220–226.
[17] M. Law, H. Kind, B. Messer, F. Kim, D. Yang, Photochemical sensing of NO_2 with SnO_2 nanoribbon nanosensors at room temperature, Angew. Chemie Int. Ed. 41 (2002) 2405–2408.
[18] J. Hu, C. Zou, Y. Su, M. Li, X. Ye, B. Cai, E. Kong, Z. Yang, Y. Zhang, Light-assisted recovery for a highly-sensitive NO_2 sensor based on RGO-CeO2 hybrids, Sens. Actuators B 270 (2018) 119–129.
[19] Y. Liu, X. Gao, F. Li, G. Lu, T. Zhang, N. Barsan, Pt-In_2O_3 mesoporous nanofibers with enhanced gas sensing performance towards ppb-level NO_2 at room temperature, Sens. Actuators B 260 (2018) 927–936.
[20] B. Zhang, G. Liu, M. Cheng, Y. Gao, L. Zhao, S. Li, F. Liu, X. Yan, T. Zhang, P. Sun, G. Lu, The preparation of reduced graphene oxide-encapsulated α-Fe_2O_3 hybrid and its outstanding NO_2 gas sensing properties at room temperature, Sens. Actuators B 261 (2018) 252–263.
[21] M. Li, J. Luo, C. Fu, H. Kan, Z. Huang, W. Huang, S. Yang, J. Zhang, J. Tang, Y. Fu, H. Li, H. Liu, PbSe quantum dots-based chemiresistors for room-temperature NO_2 detection, Sens. Actuators B 256 (2018) 1045–1056.
[22] H. Yu, T. Yang, Z. Wang, Z. Li, Q. Zhao, M. Zhang, p-N heterostructural sensor with SnO-SnO_2 for fast NO_2 sensing response properties at room temperature, Sens. Actuators B 258 (2018) 517–526.
[23] J. Zhang, D. Hu, S. Tian, Z. Qin, D. Zeng, C. Xie, $CuInS_2$ QDs decorated ring-like NiO for significantly enhanced room-temperature NO_2 sensing performances via effective interfacial charge transfer, Sens. Actuators B 256 (2018) 1001–1010.
[24] Z. Wang, T. Zhang, T. Han, T. Fei, S. Liu, G. Lu, Oxygen vacancy engineering for enhanced sensing performances: a case of SnO_2 nanoparticles-reduced graphene oxide hybrids for ultrasensitive ppb-level room-temperature NO_2 sensing, Sens. Actuators B 266 (2018) 812–822.
[25] H. Ma, L. Yu, X. Yuan, Y. Li, C. Li, M. Yin, X. Fan, Room temperature photoelectric NO_2 gas sensor based on direct growth of walnut-like In_2O_3 nanostructures, J. Alloys. Compd. 782 (2019) 1121–1126.
[26] M. Reddeppa, S. Mitta, B. Park, S. Kim, S. Park, M. Kim, DNA-CTMA functionalized GaN surfaces for NO_2 gas sensor at room temperature under UV illumination, Org. Electron. 65 (2019) 334–340.
[27] J. Wang, M. Yu, X. Li, Y. Xi, UV-enhanced NO_2 gas sensing properties of polystyrene sulfonate functionalized ZnO nanowires at room temperature, Inorg. Chem. Front. 6 (2019) 176–183.
[28] Y. Zhou, C. Zou, X. Lin, Y. Guo, UV light activated NO_2 gas sensing based on Au nanoparticles decorated few-layer MoS_2 thin film at room temperature, Appl. Phys. Lett. 113 (2018) 082103.

[29] F. Saboor, T. Ueda, K. Kamada, T. Hyodo, Y. Mortazavi, A. Khodadadi, Y. Shimizu, Enhanced NO$_2$ gas sensing performance of bare and Pd-loaded SnO$_2$ thick film sensors under UV-light irradiation at room temperature, Sens. Actuators B 223 (2016) 429–439.

[30] E. Espid, F. Taghipour, Development of highly sensitive ZnO/In$_2$O$_3$ composite gas sensor activated by UV-LED, Sens. Actuators B 241 (2017) 828–839.

[31] J. Hu, C. Zou, Y. Su, M. Li, Y. Han, E. Kong, Z. Yang, Y. Zhang, An ultrasensitive NO$_2$ gas sensor based on a hierarchical Cu$_2$O/CuO mesocrystal nanoflower, J. Mater. Chem. A 6 (2018) 17120–17131.

[32] S. Park, S. An, Y. Mun, C. Lee, UV-enhanced NO$_2$ gas sensing properties of SnO$_2$-core/ZnO-shell nanowires at room temperature, ACS Appl. Mater. Interfaces 5 (2013) 4285–4292.

[33] Z. Wang, G. Men, R. Zhang, F. Gu, D. Han, Pd loading induced excellent NO$_2$ gas sensing of 3DOM In$_2$O$_3$ at room temperature, Sens. Actuators B 263 (2018) 218–228.

[34] X. Sun, H. Hao, H. Ji, X. Li, S. Cai, C. Zheng, Nanocasting synthesis of In$_2$O$_3$ with appropriate mesostructured ordering and enhanced gas-sensing property, ACS Appl. Mater. Interfaces 4 (2014) 401–409.

[35] A. Ilin, M. Martyshov, E. Forsh, P. Forsh, M. Rumyantseva, A. Abakumov, A. Gaskov, P. Kashkarov, UV effect on NO$_2$ sensing properties of nanocrystalline In$_2$O$_3$, Sens. Actuators B 231 (2016) 491–496.

[36] T. Wang, Q. Yu, S. Zhang, X. Kou, P. Sun, G. Lu, Rational design of 3D inverse opal heterogeneous composite microspheres as excellent visible-light-induced NO$_2$ sensors at room temperature, Nanoscale 10 (2018) 4841–4851.

[37] L. Wang, Y. Kang, X. Liu, S. Zhang, W. Huang, S. Wang, ZnO nanorod gas sensor for ethanol detection, Sens. Actuators B 162 (2012) 237–243.

[38] G. Lu, J. Xu, J. Sun, Y. Yu, Y. Zhang, F. Liu, UV-enhanced room temperature NO$_2$ sensor using ZnO nanorods modified with SnO$_2$ nanoparticles, Sens. Actuators B 162 (2012) 82–88.

[39] J. Wang, X. Li, Y. Xia, S. Komarneni, H. Chen, J. Xu, L. Xiang, D. Xie, Hierarchical ZnO nanosheet-nanorod architectures for fabrication of Poly(3-hexylthiophene)/ZnO hybrid NO$_2$ sensor, ACS Appl. Mater. Interfaces 8 (2016) 8600–8607.

[40] S. Brahma, C. Yang, C. Wu, F. Chang, T. Wu, C. Huang, K. Lo, The optical response of ZnO nanorods induced by oxygen chemisorption and desorption, Sens. Actuators B 259 (2018) 900–907.

[41] D. Wei, W. Jiang, H. Gao, X. Chuai, F. Liu, F. Liu, P. Sun, X. Liang, Y. Gao, X. Yan, G. Lu, Facile synthesis of La-doped In$_2$O$_3$ hollow microspheres and enhanced hydrogen sulfide sensing characteristics, Sens. Actuators B 276 (2018) 413–420.

[42] W. Kim, M. Choi, K. Yong, Generation of oxygen vacancies in ZnO nanorods/films and their effects on gas sensing properties, Sens. Actuators B 209 (2015) 989–996.

[43] T. Hyodo, K. Urata, K. Kamada, T. Ueda, Y. Shimizu, Semiconductor-type SnO$_2$-based NO$_2$ sensors operated at room temperature under UV-light irradiation, Sens. Actuators B 253 (2017) 630–640.

[44] Y. Wang, Y. Li, K. Yu, Z. Zhu, Controllable synthesis and field emission enhancement of Al$_2$O$_3$ coated In$_2$O$_3$ core-shell nanostructures, J. Phys. D: Appl. Phys. 44 (2011) 105301.

[45] C. Zhang, X. Geng, J. Li, Y. Luo, P. Lu, Role of oxygen vacancy in tuning of optical, electrical and NO$_2$ sensing properties of ZnO$_{1-x}$ coatings at room temperature, Sens. Actuators B 248 (2017) 886–893.

Hongtao Wang received his bachelor's degree in 2016 in chemical engineering and technology from Changchun University of Technology, China. He is currently studying for degree of doctor at Jilin University. His work is studying photoelectric gas-sensing based on metal oxide nanomaterials.

Linsheng Zhou received the BS degree in Department of Electronic Science and Technology in 2017. He is currently studying for his M.E Sci degree in College of Electronic Science and Engineering, Jilin University, China.

Yueying Liu received the BS degree in Department of Micro-Electronics in 2017. She is currently studying for her M.E Sci degree in College of Electronic Science and Engineering, Jilin University, China.

Fengmin Liu received the BE degree in Department of Electronic Science and Technology in 2000. She received his Doctor's degree in College of Electronic Science and Engineering at Jilin University in 2005. Now she is a professor in Jilin University, China. Her current research is preparation and application of semiconductor oxide, especial in gas sensor and solar cell.

Xishuang Liang received the BE degree in Department of Electronic Science and Technology in 2004. He received his Doctor's degree in College of Electronic Science and Engineering at Jilin University in 2009. Now he is an associate professor of Jilin University, China. His current research is solid electrolyte gas sensor.

Fangmeng Liu received his PhD degree in 2017 from College of Electronic Science and Engineering, Jilin University, China. Now he is a lecturer of Jilin University, China. His current research interests include the application of functional materials and development of solid state electrolyte gas sensor and flexible device.

Yuan Gao received her PhD degree from Department of Analytical Chemistry at Jilin University in 2012. Now she is an associate professor in Jilin University, China. Her current research is focus on the preparation and application of graphene and semiconductor oxide, especial in gas sensor and biosensor.

Xu Yan received his M.S degree in 2013 from Nanjing Agricultural University. He joined the group of Prof. Xingguang Su at Jilin University and received his Ph.D. degree in June 2017. Since then, he did postdoctoral work with Prof. Geyu Lu and Prof. Junqiu Liu. Currently, his research interests mainly focus on the development of the functional nanomaterials for chem/bio sensors.

Geyu Lu received the B.Sci. degree in Electronic Sciences in 1985 and the M.Sci. degree in 1988 from Jilin University in China and the Dr.Eng. degree in 1998 from Kyushu University in Japan. Now he is a professor of Jilin University, China. His current research interests include the development of chemical sensors and the application of the function materials.